Theoretical Analysis of Microcavity Simultons Reinforced by $\chi^{(2)}$ and $\chi^{(3)}$ Nonlinearities

Yulei Ding, Ziqi Wei, Yifei Wang, Changxi Yang, and Chengying Bao*
State Key Laboratory of Precision Measurement Technology and Instruments, Department of Precision Instruments, Tsinghua University, Beijing 100084, China

(Received 27 March 2023; accepted 27 November 2023; published 4 January 2024)

High-Q microcavities with quadratic and cubic nonlinearities add lots of versatility in controlling microcombs. Here, we study microcavity simulton and soliton dynamics reinforced by both $\chi^{(2)}$ and $\chi^{(3)}$ nonlinearities in a continuously pumped microcavity. Theoretical analysis based on the Lagrangian approach reveals the soliton peak power and gain-loss balance are impacted by the flat part of the intracavity pump, while the dark-pulse part of the pump leads to a nearly constant soliton group velocity change. We also derived a soliton conversion efficiency upper limit that is fully determined by the coupling condition and the quantum-limited soliton timing jitter in the $\chi^{(2,3)}$ system. Numerical simulations confirm the analytical results. Our theory is particularly useful for investigating AlN microcombs and sheds light on the interplay between $\chi^{(2)}$ and $\chi^{(3)}$ nonlinearities within microcavity simultons.

DOI: 10.1103/PhysRevLett.132.013801

Introduction.—Optical simultons are two-color bright-dark soliton pairs that were first introduced in a synchronously pumped $\chi^{(2)}$ optical parametric oscillator (OPO) [1]. Recent experiments show that a similar soliton compound is possible in continuously pumped high-Q AlN microcavities [2], which is termed as microcavity simulton in this Letter. It constitutes another form of microcombs in addition to the dissipative Kerr soliton (DKS) microcombs [3–7]. DKSs have shown great prospects for the photonic chip-based optical frequency synthesizer [8], optical clock [9], LiDAR [10], spectrometer [11] and computation processor [12,13]. However, the low pump-to-soliton conversion efficiency represents an Achilles's heel for them [14–16]. Microcavity simulton offers a viable solution to improve the efficiency [2].

By pumping a microcavity at a frequency of 2ω properly, a bright soliton can arise around ω, and the pump becomes dark-pulse-like, forming the microcavity simulton [see Fig. 1(a)]. The formation of the bright soliton needs the coexistence of $\chi^{(2)}$ and $\chi^{(3)}$ nonlinearities [2]. Hence, its dynamics differs from solitons sustained by pure $\chi^{(3)}$ [4,17,18] or $\chi^{(2)}$ [1,19,20] nonlinearity, and it is referred to as a $\chi^{(2,3)}$ soliton here. Pure $\chi^{(2)}$ comb generation by pumping cavities at 2ω continuously has been investigated experimentally and theoretically [21–31], but soliton generation remains a technical challenge [26]. Most studies have focused on lithium niobate (LN) microcavities with a relatively strong $\chi^{(2)}$ effect. It needs a very high pump power (tens of kW for a LN microcavity with a Q-factor of 10^7 predicted in Ref. [32]) to observe the interplay between $\chi^{(2)}$ and $\chi^{(3)}$ nonlinarities. The intermediate $\chi^{(2)}$ nonlinearity makes AlN microcavities a versatile platform to study $\chi^{(2,3)}$ solitons and microcavity simultons [2,33]. However, analytical study on their dynamics is rare, to our knowledge.

Here, we propose a pair of Ansätze for both the signal and the pump for the microcavity simulton, which enable us to analyze the nonlinear dynamics analytically by the Lagrangian approach [34–36]. Our work reveals that the interaction within the microcavity simulton via the $\chi^{(2)}$ nonlinearity contributes to balancing phase detuning from the resonance and governs the scaling of soliton peak power and pulse width. Analysis of the gain-loss balance reveals a soliton conversion efficiency limit depending on the coupling condition only. We also derived the impact of the coexistence of $\chi^{(2)}$ and $\chi^{(3)}$ nonlinearities on soliton group velocity and quantum-limited timing jitter [36–39]. Our work can contribute to tailoring chip-based $\chi^{(2,3)}$ microcombs in doubly resonant conditions. It can also inspire work on soliton dynamics in singly resonant, parametrically driven fiber cavities [40], dichromatically pumped $\chi^{(3)}$ microcavities hosting bright-dark solitons [41], and simulton $\chi^{(2)}$ OPOs [1,42].

Ansätze for simultons.—The microcavity simulton dynamics can be modeled by the following coupled generalized Lugiato-Lefever equations [2,30,32,43,44]:

$$\frac{\partial A}{\partial T}=\left[-\frac{\kappa_1}{2}-i\delta\omega_1-i\frac{\beta_{21}L}{2T_R}\frac{\partial^2}{\partial t^2}\right]A+i\frac{L}{T_R}\left[\left(\gamma_1|A|^2+2\gamma_1|B|^2\right)A+gBA^*\right], \tag{1}$$

 © 2024 American Physical Society

$$\frac{\partial B}{\partial T}=\left[-\frac{\kappa_2}{2}-i\left(2\delta\omega_1+\frac{\delta\beta_0 L}{T_R}\right)-\frac{\delta\beta_1 L}{T_R}\frac{\partial}{\partial t}-i\frac{\beta_{22}L}{2T_R}\frac{\partial^2}{\partial t^2}\right]B+i\frac{L}{T_R}\left[\left(\gamma_2|B|^2+2\gamma_2|A|^2\right)B+gA^2\right]+\sqrt{\frac{\kappa_{2e}}{T_R}}B_{\mathrm{in}}, \quad (2)$$

where A and B are the envelopes of the intracavity fields for signal and pump (normalized so that $|A|^2$ and $|B|^2$ represent optical power), respectively; T and t are slow time and fast time; L is the cavity length; T_R is the round trip time; $\kappa_{1(2)}$ is the total loss rate for the signal (pump); κ_{2e} is the external coupling rate for the pump B_{in}; $\delta\omega_1$ is the frequency detuning for the signal; g is the $\chi^{(2)}$ nonlinearity coefficient; $\gamma_{1(2)}$ are the $\chi^{(3)}$ nonlinearity coefficients (note that we omitted the influence of mode overlap when calculating the nonlinear coefficients for cross-phase-modulation); $\delta\beta_0$ and $\delta\beta_1$ represent the phase mismatching and the group velocity mismatching, respectively; and $\beta_{21(2)}$ is the group velocity dispersion at the signal (pump) frequency.

We first used the following cavity parameters: $L=0.4$ mm, $T_R=2.8$ ps, $\kappa_1=\kappa_2/4=\kappa_{2e}/2=2\pi\times0.65$ GHz, $g=40\ \mathrm{W}^{-1/2}/\mathrm{m}$, $\gamma_1=0.75\ (\mathrm{Wm})^{-1}$, $\gamma_2=1.5\ (\mathrm{Wm})^{-1}$, $\delta\beta_1=0.4$ ps/mm, $\beta_{21}=-50\ \mathrm{fs}^2/\mathrm{mm}$, $\beta_{22}=50\ \mathrm{fs}^2/\mathrm{mm}$ for simulation. These parameters are possible for AlN microcavities with a design similar to Ref. [45]. We assumed a phase-matched condition ($\delta\beta_0=0\ \mathrm{m}^{-1}$), which can be realized by intermode phase matching [45]. A microcavity simulton can be generated from noise by scanning $\delta\omega_1$ from $-\kappa_1$ to κ_1 linearly within a slow time slot $[0,46]/\kappa_1$, and holding it at κ_1 afterward with $B_{\mathrm{in}}^2=50$ mW. A bright soliton starts to form with $\delta\omega_1$ around $\kappa_1/2$ after passing a chaotic regime [Fig. 1(b)]. Meanwhile, the pump develops a sawtoothlike waveform. Microcavity simultons also exist with slight phase mismatching (see the Supplemental Material, Sec. 3 [46–48]).

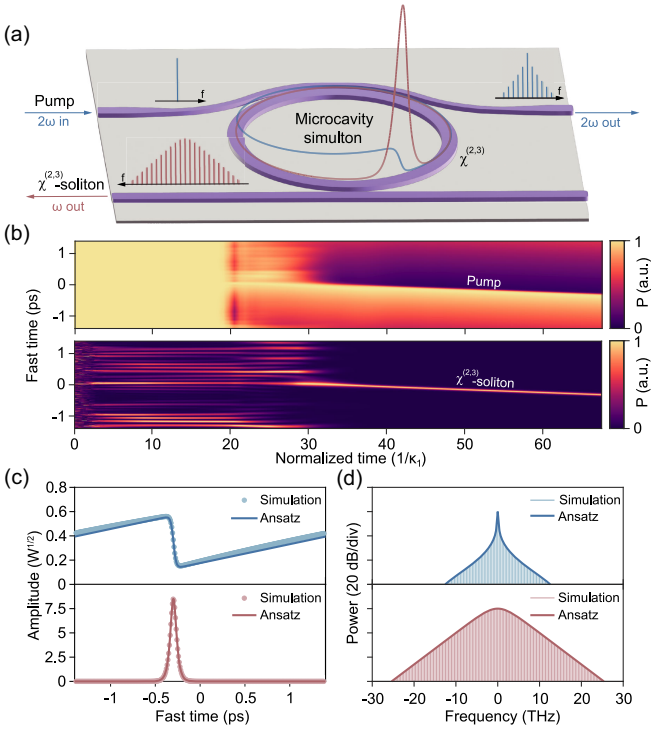

FIG. 1. (a) An illustration of $\chi^{(2,3)}$ solitons and simulton generation in a microcavity. (b) Normalized intracavity pump and signal dynamics in the simulation when scanning $\delta\omega_1$ from $-\kappa_1$ to κ_1 linearly from the beginning to $46/\kappa_1$ and holding it at κ_1 afterward. (c) Simulated amplitude of the pump and signal fields (points) and the corresponding Ansätze (curves). (d) Theoretical comb spectra derived from the Ansätze also agree with the simulation.

The simulated $\chi^{(2,3)}$ soliton still has a sech-pulse shape [Fig. 1(c)], and we used the following formulas as Ansätze for the doubly resonant signal and pump fields:

$$A=B_1\mathrm{sech}[((t-t_0)/\tau_s]\exp[-i\Omega_1(t-t_0)+i\varphi_1], \quad (3)$$

$$B=\frac{igB_1^2\tau_s}{\delta\beta_1}\tanh\left(\frac{t-t_0}{\tau_s}\right)e^{-2i\Omega_1(t-t_0)+2i\varphi_1}-\frac{2igB_1^2\tau_s}{\delta\beta_1 T_R}(t-t_0)e^{-2i\Omega_1(t-t_0)+2i\varphi_1}+B_2e^{i\varphi_2}, \quad (4)$$

where B_1, t_0, τ_s, Ω_1, and φ_1 are the amplitude, timing, pulse width, center frequency shift, and phase of the soliton, respectively. The Ansätze in Eq. (4) can be derived by substituting A into Eq. (2), and a linear term is added to satisfy the periodic boundary condition, i.e., $B(-T_R/2)=B(T_R/2)$ (see the Supplemental Material, Sec. 1 [46]). B_2 and φ_2 in Eq. (4) are the amplitude and phase of the flat part for the intracavity pump field. The Ansätze for A and B agree reasonably with the simulation [Fig. 1(c)]. Since the linear term was added for the periodic condition rather than rigorously derived, it causes a slight discrepancy between B and the simulation. The amplitude for the pump in the microcavity simulton is asymmetric, while the simulton amplitude in a $\chi^{(2)}$ OPO is symmetric (tanh-shaped) without a flat part [1]. The flat part and asymmetry of the pump field will impact the $\chi^{(2,3)}$ soliton dynamics via the $\chi^{(2)}$ nonlinearity. Equation (4) shows that group velocity mismatch ($\delta\beta_1$), plays an important role in shaping the microcavity simulton.

In the frequency domain, the signal comb has a smooth sech^2 shape without a dominant line, as the pump is in the 2ω band [Fig. 1(d)]. There is a steep decrease in $|B|$ when it overlaps with the soliton pulse. Owing to this modulation, the pump also develops a comb in the 2ω band. The simulated pump and signal combs agree with the Ansätze determined comb shapes [Fig. 1(d)], which further validates our Ansätze.

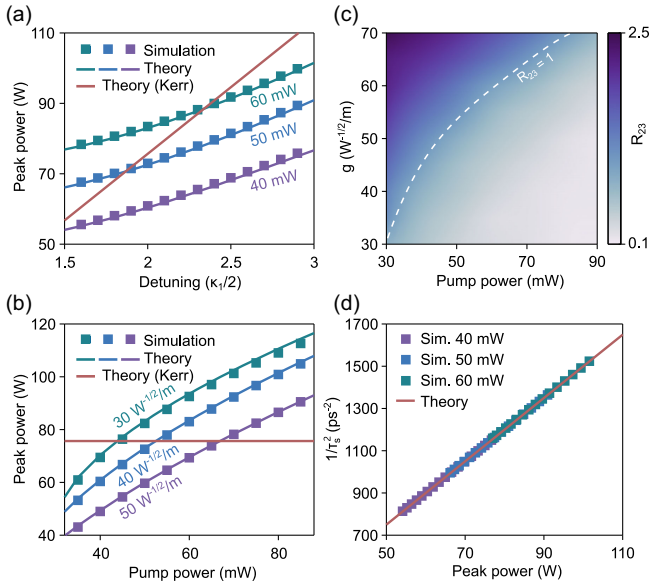

FIG. 2. The change of soliton peak power versus (a) detuning $\delta\omega_1$ and (b) pump power B_{in}^2. (c) Comparison between $\chi^{(2)}$ and $\chi^{(3)}$ nonlinear phase shift. (d) Soliton pulse width still has an inverse relationship with the soliton amplitude B_1. Square colors stand for pump powers in panels (a),(d) and g in panel (b).

Soliton peak power and pulse width.—With these Ansätze, we analyzed the $\chi^{(2,3)}$ soliton dynamics by the Lagrangian approach based on Eq. (1) [34–36]. Details of the method can be found in the Supplemental Material, Sec. 1 [46]. We first analyzed the peak power (B_1^2) of the $\chi^{(2,3)}$ soliton, whose scaling law is derived to be

$$\delta\omega_1 T_R = \gamma_1 B_1^2 L/2 + gB_2 L\cos(2\varphi_1 - \varphi_2). \tag{5}$$

This means the round trip phase detuning $\delta\omega_1 T_R$ is balanced by nonlinear phase accumulation from both the $\chi^{(3)}$ and the $\chi^{(2)}$ nonlinearities [49]. Since the $\chi^{(3)}$ nonlinearity induced round trip phase shift for a soliton is $\gamma_1 B_1^2 L/2$, the peak power for a DKS scales as $\gamma_1 B_1^2 L = 2\delta\omega_1 T_R$ [3,49,50]. The flat part of B also contributes to the nonlinear phase accumulation via the $\chi^{(2)}$ nonlinearity for $\chi^{(2,3)}$ solitons. Therefore, the simulated soliton peak power no longer changes linearly with $\delta\omega_1$ and is in excellent agreement with Eq. (5) [see Fig. 2(a), where B_2 and φ_2 were determined by the simulated B at $t = t_0$]. The simulated soliton peak power increases with pump power for a fixed detuning. This increase was further analyzed in Fig. 2(b) with $\delta\omega_1 = \kappa_1$. The simulated soliton peak power change versus pump power is also in excellent agreement with Eq. (5) (DKS peak power is almost independent from the pump power [50]). Furthermore, when g increases, the soliton peak power decreases, also consistent with Eq. (5). We further defined $R_{23} = 2gB_2 L\cos(2\varphi_1 - \varphi_2)/\gamma_1 B_1^2 L$ as a measure of the relative strength of $\chi^{(2)}$ and $\chi^{(3)}$ nonlinearities. For a given g and pump power, we scanned $\delta\omega_1$ to have the maximum R_{23} as plotted in Fig. 2(c), which clearly shows their comparable strength. It needs appropriate (not large) g and pump power to have comparable $\chi^{(2)}$ and $\chi^{(3)}$ effects and $\chi^{(2,3)}$ soliton. The used pump power is much lower than the critical power (6 W) predicted in Ref. [32], as the soliton endows a high peak power. The microcavity simulton ceases to exist for a very large g or a very small γ_1.

Pulse width τ_s is shown to follow the relationship

$$B_1^2\tau_s^2 = -\beta_{21}/\gamma_1. \tag{6}$$

Hence, the soliton area theorem (the product of soliton amplitude and duration is a constant) [51] is retained for $\chi^{(2,3)}$ solitons in doubly resonant microcavities. Figure 2(d) verifies the relationship under different soliton peak powers (obtained by changing B_{in} and $\delta\omega_1$).

Gain-loss balance and soliton efficiency.—We further analyzed the dissipation dynamics of $\chi^{(2,3)}$ solitons. The soliton energy can be calculated as $E = 2B_1^2\tau_s$, whose motion equation is (see the Supplemental Material, Sec. 1 [46])

$$\frac{dE}{dT} = -\kappa_1 E + \frac{2gLB_2\sin(2\varphi_1 - \varphi_2)E}{T_R}. \tag{7}$$

The second term on the right-hand side of Eq. (7) can be regarded as the parametric gain via the $\chi^{(2)}$ nonlinearity and it is the flat part of the pump that contributes to the gain-loss balance of the $\chi^{(2,3)}$ soliton. Although the $\chi^{(3)}$ nonlinearity enables energy exchange within the ω band, it does not add to the net parametric gain. The relationship is verified in Fig. 3(a). Hence, $2\varphi_1 - \varphi_2$ should fall in $(0, \pi)$ and $B_2 \geq \kappa_1 T_R/2gL$.

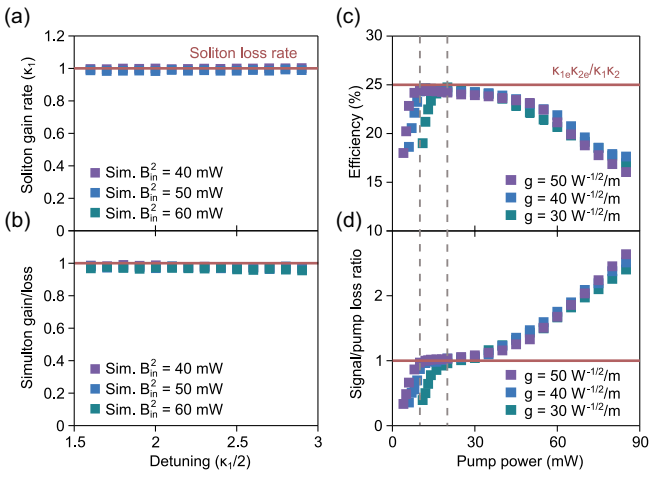

FIG. 3. (a) $\chi^{(2)}$ parametric gain rate for the soliton based on Eq. (7) with $g = 40\ \text{W}^{-1/2}/\text{m}$. (b) Round trip gain-loss ratio $2\sqrt{\kappa_{2e}T_R}B_2 B_{\text{in}}\cos\varphi_2/(\kappa_1 E + \kappa_2 B_2^2 T_R)$ for microcavity simultons under different detunings. (c) Maximum simulated soliton conversion efficiencies are clamped by Eq. (9). (d) Ratio of round trip loss for signal and pump under the maximum soliton efficiency.

Considering the gain-loss balance for the microcavity simulton instead of the $\chi^{(2,3)}$ soliton, the round trip gain from external coupling of $B_{\rm in}$ should equal the round trip loss for the simulton, which means

$$\left|B+\sqrt{\kappa_{2e}T_R}B_{\rm in}\right|^2-|B|^2=2\sqrt{\kappa_{2e}T_R}B_2B_{\rm in}\cos\varphi_2 =\kappa_1E+\kappa_2B_2^2T_R\geq 2B_2\sqrt{\kappa_1\kappa_2ET_R}. \tag{8}$$

The first two formulas represent round trip gain from the external pump, and the third represents the round trip loss (flat part of B dominates the intracavity pump energy). The gain-loss balance for the microcavity simulton is verified in Fig. 3(b). The equal sign in Eq. (8) is reached when the round trip loss for the signal equals that of the pump. According to Eq. (8), a limit for pump-to-soliton conversion efficiency η is derived as

$$\eta=\frac{\kappa_{1e}E}{B_{\rm in}^2}\leq\frac{\kappa_{1e}\kappa_{2e}\cos^2\varphi_2}{\kappa_1\kappa_2}\leq\frac{\kappa_{1e}\kappa_{2e}}{\kappa_1\kappa_2}, \tag{9}$$

where κ_{1e} is the external coupling rate for the signal. The simulated maximum η (obtained with the maximum $\delta\omega_1$) for different pump powers and g is shown in Fig. 3(c) for a critically coupled cavity for both 2ω and ω bands, and is clamped by Eq. (9) at 25%. Figure 3(d) confirms that the maximum efficiency is reached when the loss of the signal is equal to that of the pump. Distinct from continuously pumped DKSs whose efficiency is proportional to τ_s/T_R [15], $\chi^{(2,3)}$ solitons have an efficiency limit that is independent from soliton profiles. Based on the coupling conditions given in Ref. [45] (the same sample used in Ref. [2]), the maximum η is 20%, while the measured highest efficiency is 17% [2] (wavelength-dependent coupling may cause the slight discrepancy).

Group velocity and quantum-limited timing jitter.—Group velocity (v_g) and soliton timing which determine the comb frequency stability [6,52] are also impacted by the modulated pump. The derived motion of the $\chi^{(2,3)}$ soliton timing t_0 in the retarded time frame is

$$\frac{dt_0}{dT}=\frac{\beta_{21}L\Omega_1}{T_R}-\frac{g^2LB_1^2\tau_s^2}{\delta\beta_1T_R}-\frac{\pi^2\cos(2\varphi_1-\varphi_2)gL\Omega_1B_2\tau_s^2}{3T_R} +\frac{\pi^2g^2LB_1^2\tau_s^3}{3\delta\beta_1T_R^2}\approx-\frac{g^2LB_1^2\tau_s^2}{\delta\beta_1T_R}\approx\frac{g^2L\beta_{21}}{\delta\beta_1\gamma_1T_R}. \tag{10}$$

The four terms on the right-hand side represent group velocity change (δv_g, $\delta v_g/v_g=-dt_0/dT$) induced by the center frequency shift Ω_1 via dispersion, and the tanh part, the flat part, and the linear part of B via the $\chi^{(2)}$ nonlinearity, respectively. The second term, which agrees with the previous work on soliton group velocity change in $\chi^{(2)}$ OPOs and is proportional to $1/\delta\beta_1$ ($\delta\beta_1$ affects amplitude of the tanh part) [1,53], was found to dominate. Although

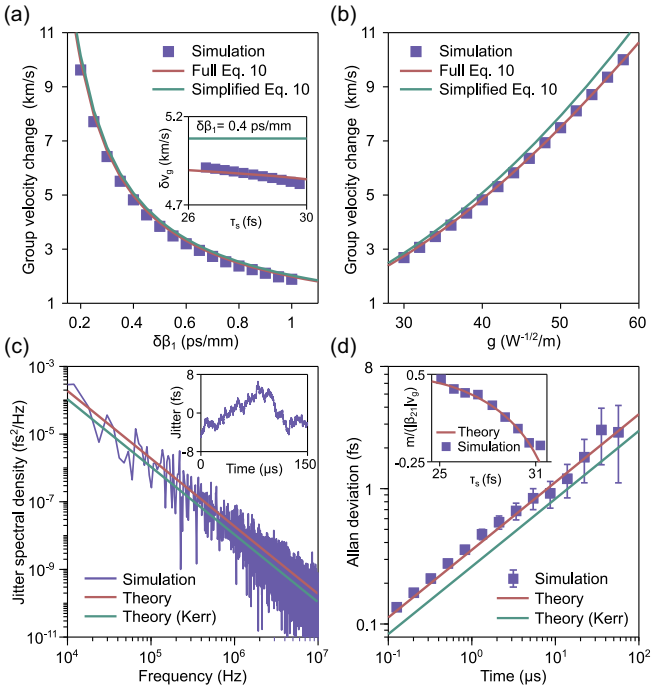

FIG. 4. (a) Simulated δv_g decreases inversely with $\delta\beta_1$, and the inset shows δv_g changes slightly with τ_s. (b) Simulated δv_g increases quadratically with g. (c) Simulated and theoretical jitter spectral density with the inset showing the simulated soliton random walk. (d) Allan deviation of the simulated and theoretical quantum-limited timing jitter. The inset shows the simulated and theoretical m as τ_s increases.

$\chi^{(3)}$ nonlinearity does not impact δv_g directly, Eq. (10) shows that δv_g for $\chi^{(2,3)}$ soliton is insensitive to change in $\delta\omega_1$ and τ_s due to the presence of $\chi^{(3)}$ nonlinearity and the retained soliton area theorem.

The inverse relationship between δv_g and $\delta\beta_1$ is validated in Fig. 4(a). The simulated δv_g with increasing $\delta\beta_1$ (under $\delta\omega_1=\kappa_1$ and $B_{\rm in}^2=50$ mW) agrees well with the full and simplified Eq. (10). δv_g will decrease slightly with τ_s when varying $\delta\omega_1$. It is mainly the fourth term in Eq. (10) resulting from the linear part of B that contributes to the decrease [inset of Fig. 4(a)]. When increasing g in the simulation, δv_g would increase nearly quadratically, as Eq. (10) predicts [Fig. 4(b)]. The deviation from the simplified Eq. (10) becomes larger with increasing g, since $B_1^2\tau_s^2$ starts to deviate from $|\beta_{21}|/\gamma_1$ under stronger $\chi^{(2)}$ nonlinearity (see the Supplemental Material, Sec. 3 [46]).

Then we analyzed the impact of the group velocity change on quantum-limited soliton timing jitter [36,37]. The derived quantum-limited timing jitter spectral density for a $\chi^{(2,3)}$ soliton is (see the Supplemental Material, Sec. 2 [46])

$$S_{t0}(\omega_0)=\frac{\hbar\omega\kappa_1}{E\omega_0^2}\left[\frac{\pi^2\tau_s^2}{12}+\frac{(\beta_{21}v_g-m)^2}{3\tau_s^2(\omega_0^2+\kappa_1^2)}-\frac{\omega_0(\beta_{21}v_g-m)}{\omega_0^2+\kappa_1^2}\right], \tag{11}$$

where $m = \pi^2\tau_s^2 g L B_2 \cos(2\varphi_1 - \varphi_2)/3T_R$ and ω_0 is the Fourier frequency. If $g = 0\ \mathrm{W}^{-1/2}/\mathrm{m}$, m vanishes and Eq. (11) reduces to the quantum-limited timing jitter for DKSs.

The simulated jitter spectral density (see Ref. [37] and the Supplemental Material, Sec. 2 [46], for methods) is in good agreement with the theory as shown in Fig. 4(c) and is about 1.76 times of the DKS theory due to a positive m for $\delta\omega_1 = 3.5\kappa_1/2$ and $B_{\mathrm{in}}^2 = 50$ mW. The inset shows the simulated random walk of the soliton timing, which was used to calculate the Allan deviation for the soliton diffusion [37]. The simulation is also in excellent agreement with the theory and is about 1.33 times of the theoretical DKS quantum diffusion [Fig. 4(d)]. Similar to DKSs, the timing jitter is still dominated by fluctuation of the center frequency shift Ω_1 [second term in Eq. (11)], but this fluctuation can further penetrate into jitter via $\chi^{(2)}$ nonlinearity by the flat part of B and nonzero m besides dispersion β_{21} [see the third term in Eq. (10)]. The inset shows the simulated and theoretical m versus τ_s when varying $\delta\omega_1$. It shows the additional noise from the $\chi^{(2)}$ nonlinearity is relatively large for short solitons or large $\delta\omega_1$ and starts to decrease or even becomes negative when $\delta\omega_1$ decreases (meanwhile B_1^2 and η will decrease). Finally, the omitted narrow band AlN Raman gain [54] does not impact δv_g and quantum-limited timing jitter strongly (see the Supplemental Material, Sec. 3 [46]).

Conclusion.—We have studied the simulton dynamics formed in microcavities with comparable $\chi^{(2)}$ and $\chi^{(3)}$ nonlinearities. The interaction within a microcavity simulton via the $\chi^{(2)}$ nonlinearity impacts the soliton peak power, dissipation dynamics, group velocity, and quantum-limited timing jitter of $\chi^{(2,3)}$ solitons (thus, their applications in precision measurements). The highest soliton efficiency is realized when the loss for the signal equals the pump. These $\chi^{(2,3)}$ solitons can enable midinfrared microcomb generation by pumping at the telecom band. Moreover, the impacts of Hopf bifurcation [55–59], active gain [60,61], and quantum dynamics [36,37,62–64] on microcavity simultons and $\chi^{(2,3)}$ systems is worth investigation in the near future.

This work is supported by the National Natural Science Foundation of China (62250071, 62175127), by the National Key Research and Development Program of China (2021YFB2801200), by the Tsinghua University Initiative Scientific Research Program (20211080080, 20221080069), and by the Tsinghua-Toyota Joint Research Fund. We acknowledge discussions with Jin-Yu Liu at Caltech.

*cbao@tsinghua.edu.cn

[1] M. Jankowski, A. Marandi, C. R. Phillips, R. Hamerly, K. A. Ingold, R. L. Byer, and M. Fejer, Phys. Rev. Lett. **120**, 053904 (2018).
[2] A. W. Bruch, X. Liu, Z. Gong, J. B. Surya, M. Li, C.-L. Zou, and H. X. Tang, Nat. Photonics **15**, 21 (2021).
[3] T. Herr, V. Brasch, J. D. Jost, C. Y. Wang, N. M. Kondratiev, M. L. Gorodetsky, and T. J. Kippenberg, Nat. Photonics **8**, 145 (2014).
[4] T. J. Kippenberg, A. L. Gaeta, M. Lipson, and M. L. Gorodetsky, Science **361**, eaan8083 (2018).
[5] A. L. Gaeta, M. Lipson, and T. J. Kippenberg, Nat. Photonics **13**, 158 (2019).
[6] S. A. Diddams, K. Vahala, and T. Udem, Science **369**, eaay3676 (2020).
[7] L. Chang, S. Liu, and J. E. Bowers, Nat. Photonics **16**, 95 (2022).
[8] D. T. Spencer, T. Drake, T. C. Briles, J. Stone, L. C. Sinclair, C. Fredrick, Q. Li, D. Westly, B. R. Ilic, A. Bluestone *et al.*, Nature (London) **557**, 81 (2018).
[9] Z. L. Newman, V. Maurice, T. Drake, J. R. Stone, T. C. Briles, D. T. Spencer, C. Fredrick, Q. Li, D. Westly, B. R. Ilic *et al.*, Optica **6**, 680 (2019).
[10] J. Riemensberger, A. Lukashchuk, M. Karpov, W. Weng, E. Lucas, J. Liu, and T. J. Kippenberg, Nature (London) **581**, 164 (2020).
[11] M.-G. Suh, Q.-F. Yang, K. Y. Yang, X. Yi, and K. J. Vahala, Science **354**, 600 (2016).
[12] X. Xu, M. Tan, B. Corcoran, J. Wu, A. Boes, T. G. Nguyen, S. T. Chu, B. E. Little, D. G. Hicks, R. Morandotti *et al.*, Nature (London) **589**, 44 (2021).
[13] J. Feldmann, N. Youngblood, M. Karpov, H. Gehring, X. Li, M. Stappers, M. Le Gallo, X. Fu, A. Lukashchuk, A. S. Raja *et al.*, Nature (London) **589**, 52 (2021).
[14] C. Bao, L. Zhang, A. Matsko, Y. Yan, Z. Zhao, G. Xie, A. M. Agarwal, L. C. Kimerling, J. Michel, L. Maleki *et al.*, Opt. Lett. **39**, 6126 (2014).
[15] X. Yi, Q.-F. Yang, K. Y. Yang, M.-G. Suh, and K. Vahala, Optica **2**, 1078 (2015).
[16] P.-H. Wang, J. A. Jaramillo-Villegas, Y. Xuan, X. Xue, C. Bao, D. E. Leaird, M. Qi, and A. M. Weiner, Opt. Express **24**, 10890 (2016).
[17] A. Hasegawa and F. Tappert, Appl. Phys. Lett. **23**, 142 (1973).
[18] P. Grelu and N. Akhmediev, Nat. Photonics **6**, 84 (2012).
[19] A. V. Buryak, P. Di Trapani, D. V. Skryabin, and S. Trillo, Phys. Rep. **370**, 63 (2002).
[20] A. Roy, R. Nehra, S. Jahani, L. Ledezma, C. Langrock, M. Fejer, and A. Marandi, Nat. Photonics **16**, 162 (2022).
[21] V. Ulvila, C. Phillips, L. Halonen, and M. Vainio, Opt. Express **22**, 10535 (2014).
[22] T. Hansson, F. Leo, M. Erkintalo, J. Anthony, S. Coen, I. Ricciardi, M. De Rosa, and S. Wabnitz, J. Opt. Soc. Am. B **33**, 1207 (2016).
[23] S. Mosca, M. Parisi, I. Ricciardi, F. Leo, T. Hansson, M. Erkintalo, P. Maddaloni, P. De Natale, S. Wabnitz, and M. De Rosa, Phys. Rev. Lett. **121**, 093903 (2018).
[24] S. Smirnov, B. Sturman, E. Podivilov, and I. Breunig, Opt. Express **28**, 18006 (2020).
[25] P. Parra-Rivas, C. Mas-Arabí, and F. Leo, Phys. Rev. A **101**, 063817 (2020).
[26] E. Podivilov, S. Smirnov, I. Breunig, and B. Sturman, Phys. Rev. A **101**, 023815 (2020).

[27] S. Smirnov, V. Andryushkov, E. Podivilov, B. Sturman, and I. Breunig, Opt. Express **29**, 27434 (2021).
[28] D. N. Puzyrev, V. V. Pankratov, A. Villois, and D. V. Skryabin, Phys. Rev. A **104**, 013520 (2021).
[29] N. Amiune, D. N. Puzyrev, V. V. Pankratov, D. V. Skryabin, K. Buse, and I. Breunig, Opt. Express **29**, 41378 (2021).
[30] D. V. Skryabin, Opt. Express **29**, 28521 (2021).
[31] M. Nie and S.-W. Huang, Opt. Lett. **45**, 2311 (2020).
[32] A. Villois, N. Kondratiev, I. Breunig, D. N. Puzyrev, and D. V. Skryabin, Opt. Lett. **44**, 4443 (2019).
[33] M. Nie, Y. Xie, and S.-W. Huang, Nanophotonics **10**, 1691 (2021).
[34] A. Hasegawa, IEEE J. Sel. Top. Quantum Electron. **6**, 1161 (2000).
[35] J. Li, C. Bao, Q.-X. Ji, H. Wang, L. Wu, S. Leifer, C. Beichman, and K. Vahala, Optica **9**, 231 (2022).
[36] A. B. Matsko and L. Maleki, Opt. Express **21**, 28862 (2013).
[37] C. Bao, M.-G. Suh, B. Shen, K. Şafak, A. Dai, H. Wang, L. Wu, Z. Yuan, Q.-F. Yang, A. B. Matsko, F. X. Kärtner, and K. J. Vahala, Nat. Phys. **17**, 462 (2021).
[38] D. Jeong, D. Kwon, I. Jeon, I. H. Do, J. Kim, and H. Lee, Optica **7**, 1108 (2020).
[39] K. Jia, X. Wang, D. Kwon, J. Wang, E. Tsao, H. Liu, X. Ni, J. Guo, M. Yang, X. Jiang *et al.*, Phys. Rev. Lett. **125**, 143902 (2020).
[40] N. Englebert, F. De Lucia, P. Parra-Rivas, C. M. Arabí, P.-J. Sazio, S.-P. Gorza, and F. Leo, Nat. Photonics **15**, 857 (2021).
[41] S. Zhang, T. Bi, G. N. Ghalanos, N. P. Moroney, L. Del Bino, and P. Del'Haye, Phys. Rev. Lett. **128**, 033901 (2022).
[42] N. Jornod, M. Jankowski, L. M. Krüger, V. J. Wittwer, N. Modsching, C. Langrock, C. R. Phillips, U. Keller, T. Südmeyer, and M. M. Fejer, Optica **10**, 826 (2023).
[43] L. A. Lugiato and R. Lefever, Phys. Rev. Lett. **58**, 2209 (1987).
[44] S. Coen, H. G. Randle, T. Sylvestre, and M. Erkintalo, Opt. Lett. **38**, 37 (2013).
[45] A. W. Bruch, X. Liu, J. B. Surya, C.-L. Zou, and H. X. Tang, Optica **6**, 1361 (2019).
[46] See Supplemental Material at http://link.aps.org/supplemental/10.1103/PhysRevLett.132.013801 for details of the Lagrangian approach and numerical simulations, and Refs. [47,48].
[47] X. Guo, C.-l. Zou, C. Schuck, H. Jung, R. Cheng, and H. X. Tang, Light Sci. Appl. **6**, e16249 (2017).
[48] F. Leo, T. Hansson, I. Ricciardi, M. De Rosa, S. Coen, S. Wabnitz, and M. Erkintalo, Phys. Rev. A **93**, 043831 (2016).
[49] C. Bao and C. Yang, Phys. Rev. A **92**, 053831 (2015).
[50] S. Coen and M. Erkintalo, Opt. Lett. **38**, 1790 (2013).
[51] G. P. Agrawal, *Nonlinear Fiber Optics* (Academic, New York, 2007), 10.1007/3-540-46629-0_9.
[52] S. T. Cundiff and J. Ye, Rev. Mod. Phys. **75**, 325 (2003).
[53] D. V. Skryabin and A. R. Champneys, Phys. Rev. E **63**, 066610 (2001).
[54] S. Yao, Z. Wei, Y. Guo, L. Zhang, J. Wang, J. Yan, C. Bao, and C. Yang, Opt. Lett. **46**, 5312 (2021).
[55] F. Leo, L. Gelens, P. Emplit, M. Haelterman, and S. Coen, Opt. Express **21**, 9180 (2013).
[56] C. Bao, J. A. Jaramillo-Villegas, Y. Xuan, D. E. Leaird, M. Qi, and A. M. Weiner, Phys. Rev. Lett. **117**, 163901 (2016).
[57] E. Lucas, M. Karpov, H. Guo, M. Gorodetsky, and T. J. Kippenberg, Nat. Commun. **8**, 736 (2017).
[58] M. Yu, J. K. Jang, Y. Okawachi, A. G. Griffith, K. Luke, S. A. Miller, X. Ji, M. Lipson, and A. L. Gaeta, Nat. Commun. **8**, 14569 (2017).
[59] X. Yi, Q.-F. Yang, K. Y. Yang, and K. Vahala, Nat. Commun. **9**, 3565 (2018).
[60] H. Bao, A. Cooper, M. Rowley, L. Di Lauro, J. S. Totero Gongora, S. T. Chu, B. E. Little, G.-L. Oppo, R. Morandotti, D. J. Moss *et al.*, Nat. Photonics **13**, 384 (2019).
[61] M. Rowley, P.-H. Hanzard, A. Cutrona, H. Bao, S. T. Chu, B. E. Little, R. Morandotti, D. J. Moss, G.-L. Oppo, J. S. Totero Gongora *et al.*, Nature (London) **608**, 303 (2022).
[62] M. A. Guidry, D. M. Lukin, K. Y. Yang, R. Trivedi, and J. Vučković, Nat. Photonics **16**, 52 (2022).
[63] Z. Yang, M. Jahanbozorgi, D. Jeong, S. Sun, O. Pfister, H. Lee, and X. Yi, Nat. Commun. **12**, 4781 (2021).
[64] M. Kues, C. Reimer, J. M. Lukens, W. J. Munro, A. M. Weiner, D. J. Moss, and R. Morandotti, Nat. Photonics **13**, 170 (2019).